

# Self-Healing and Electrical Properties of Viscoelastic Polymer–Carbon Blends

Pavel Milkin, Michael Danzer, and Leonid Ionov\*

Self-healing polymer–carbon composites are seen as promising materials for future electronic devices, which must be able to restore not only their structural integrity but also electrical performance after cracking and wear. Despite multiple reports about self-healing conductive elements, there is a lack of a broad fundamental understanding of correlation between viscoelasticity of such composites, their electrical properties, and self-healing of their mechanical as well as electrical properties. Here, it is reported through investigation of electromechanical properties of blends of carbon black (CB) as conductive filler and viscoelastic polymers (polydimethylsiloxanes (PDMS) and polyborosiloxane (PBS)) with different relaxation times as matrices. It is shown that behavior of composites depends strongly on the viscoelastic properties of polymers. Low molecular polymer composite possesses high conductivity due to strong filler network formation, quick electrical, and mechanical properties restoration, but for this the ability is sacrificed to flow and ductility at large deformation (material is brittle). In contrary, high relaxation time polymer composite behaves elastically on small time and flows at large time scale due to weak filler network and can heal. However, the electrical properties are worse than that of carbon and viscous polymer and degrade with time.

occupying an entire room to nanoscale transistors that now ensure the operation of any circuit board. One important field is wearable, flexible electronics, which can be integrated, for example, in apparel. One essential problem of flexible electronics is its robustness—materials must be able to withstand multiple cycles of bending or stretching.<sup>[1]</sup> All solid materials inevitably undergo failure after many loading/unloading cycles. As results, devices endure failure due to mechanical or electrical stress and cannot be easily repaired that contributes to the E-waste problem.<sup>[2]</sup> Furthermore, such electronics contain nondegradable polymers (polyethers, polyimide, etc.) and metals, which require proper recycling to avoid environmental pollution.<sup>[3,4]</sup> On the other hand, nature shows that living organisms can fight for survival against injuries, by repairing damaged tissues through self-healing. This ability of living organisms inspired scientists to develop materials, which are able to heal cracks after failure.

## 1. Introduction

Nowadays, electronic devices are ineradicably integrated into our everyday life. They underwent evolution from calculators

Due to this, self-healing polymers have recently attracted attention to solve the problem of degradation and failure of soft electronic devices as well as to eliminate their fragility, existing fatigue strength, and weakness of contacts with metal conductors within the time.<sup>[5–7]</sup> The self-healing may include mechanisms of autogenous healing,<sup>[8]</sup> vascular,<sup>[9]</sup> and capsule-based<sup>[10]</sup> materials, shape memory effect,<sup>[11]</sup> and reformation of different chemical bonds.<sup>[2,12,13]</sup> The last one provides unlimited self-healing capability and seems as most promising. Self-healing in such polymers goes through reactions of metal–ligand coordination,<sup>[14]</sup> H-bonding,<sup>[15]</sup>  $\pi$ – $\pi$  stacking,<sup>[16]</sup> dynamic covalent bonding,<sup>[17]</sup> etc. These mechanisms require relatively high mobility of chain segments to implement the self-healing purpose. Therefore, these not-electrically-conductive polymers, which are used in their viscoelastic state above glass transition temperature, are combined with functional fillers with electrical properties.<sup>[18,19]</sup> In such blends, the matrix and filler impart viscoelastic material properties as a combination of both, which are important to consider in various applications. In most cases, research was focused on restoration of integrity of broken objects and their mechanical properties. Restoration of other functionalities such as electrical conductivity of materials is also an important topic.<sup>[20,21]</sup>

Functionality of self-healing materials is often achieved by blending self-healing polymers and functional filler. Therefore, the understanding the matrix-filler interaction of such systems

P. Milkin, L. Ionov  
 Faculty of Engineering Sciences  
 University of Bayreuth  
 Ludwig Thoma Str. 36A, Bayreuth 95447, Germany  
 E-mail: leonid.ionov@uni-bayreuth.de

M. Danzer  
 Chair of Electrical Energy Systems  
 University of Bayreuth  
 Universitätsstr. 30, Bayreuth 95447, Germany

L. Ionov  
 Bavarian Polymer Institute  
 University of Bayreuth  
 Bayreuth 95447, Germany

 The ORCID identification number(s) for the author(s) of this article can be found under <https://doi.org/10.1002/marc.202200307>

© 2022 The Authors. Macromolecular Rapid Communications published by Wiley-VCH GmbH. This is an open access article under the terms of the Creative Commons Attribution License, which permits use, distribution and reproduction in any medium, provided the original work is properly cited.

DOI: 10.1002/marc.202200307

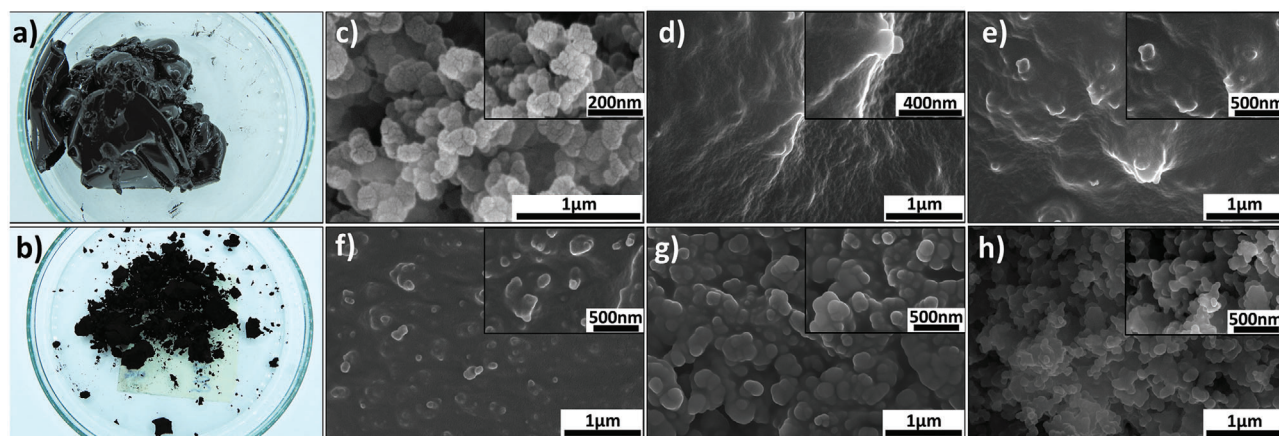


**Figure 1.** Morphology of polymer-carbon blends: a) image of PDMS 105 cSt, 5 vol% of CB. b) image of PDMS  $10^5$  cSt 20 vol% of CB. c) SEM images of prictine CB. SEM images of PDMS  $10^5$  cSt - CB composites with d) 5 vol%, e) 10 vol%, f) 15 vol%, g) 20 vol%, h) 30 vol%.

is the key to meaningful tailoring material properties. However, many papers on this topic present scarce data obtained by one or another rheological method that does not allow building a complete picture of viscoelastic properties of a viscoelastic self-healing matrix and a functional filler. As an example of a viscoelastic matrix, the Silly-Putty, PBS based material, may be considered. Several authors used composites based on PBS—and several carbon fillers (graphene, multiwalled carbon nanotubes) as a pressure sensor,<sup>[18]</sup> strain rate sensor,<sup>[22]</sup> triboelectric nanogenerator,<sup>[23]</sup> gas sensor,<sup>[24]</sup> and do demonstrate their functionality. Nevertheless, authors leave a significant block behind the scenes of the choice of polymer, its interaction with filler while providing scanty rheological investigation and demonstrating material properties out of its linear range of electrical and mechanical responses without a bit of justification of applicability and reliability of such conditions for actual devices.<sup>[25]</sup> Including the electrical characteristics are often measured at one particular voltage, assuming that Ohm's law is fulfilled in the whole voltage range. However, the volt-ampere characteristic of such materials may be nonlinear.<sup>[24,26]</sup>

In this study, we performed a thorough investigation of the influence of different PDMS/PBS polymer matrices on the electromechanical properties of carbon-based composites. In comparison to other studies, we seek to elucidate the applicability limits of such materials through detailed rheological, mechanical, and electrical investigation instead of considering any specific application field. Carbon black was chosen as a model conductive carbon filler with various concentrations. The filler-polymer interaction in such composites, the viscoelastic properties, relaxation processes, and electrical conductivity mechanisms of material are discussed.

## 2. Experimental Results

### 2.1. Pure Materials

To understand the influence of polymer on the rheological and self-healing behavior of carbon-polymer composites, we prepared blends of carbon black as conductive filler and polydimethylsiloxanes (PDMS) as a matrix with up to 30 vol%

of nanoparticles. The carbon black particles are  $\approx 48$  nm in size, according to Brunauer-Emmett-Teller analysis results, assuming spherical particles shape. As matrix material, three polydimethylsiloxane-based polymers of different molecular weights (Figure S5, Supporting Information) with various relaxation times were chosen. The first one is linear PDMS 65 cSt, which is a linear polymer with a molecular mass ( $M_w = 6.5$  kg mol<sup>-1</sup>) lower than the critical molecular mass ( $M_c = 24.5$  kg mol<sup>-1</sup><sup>[27]</sup>) when entanglements start to play an important role. The relaxation time is low and cannot be measured, the polymer behaves as Newtonian liquid. The second one is PDMS  $2 \times 10^7$  cSt, a viscoelastic polymer ( $M_w = 388$  kg mol<sup>-1</sup>) with  $\approx 32$  entanglements per chain. Its average relaxation time  $\lambda \approx 0.1$  s (Figure S5, Supporting Information), although the relaxation time peak is quite broad due to high polydispersity. Due to high polydispersity, the elastic plateau cannot be achieved but is expected to be in the range between 0.1 and 1 MPa, meaning that the polymer behaves as a melt. The third polymer—polyborosiloxane (PBS)—is a product of polycondensation of boric acid and hydroxy-terminated PDMS, creating crosslinked network due to Si-O-B bonds and supramolecular structure through hydrogen and dative Si-O-B bonds.<sup>[28]</sup> The effective degree of polymerization is about 3650 monomer units per chain which is much higher than  $\approx 90$  units per chain for the initial PDMS oligomer (Figure S1b, Supporting Information). The PBS has two relaxations times. First one is at around 1 s, which is relaxation time of polymer chain. The other relaxation process is the fast relaxation of supramolecular structure with  $\lambda \leq 10-3$  s.<sup>[28]</sup> The  $G'$  at the plateau is  $\approx 4$  kPa that is lower than that of polymer melts ( $\approx 0.5$  MPa), meaning that the polymer behaves as an entangled solution, where a solvent is initial low molecular weight PDMS. The  $G'$  of PDMS melt at the elastic plateau is  $\approx 0.5$  MPa meaning that  $G'(\text{solution})/G'(\text{melt}) = 0.01$  that gives the concentration of very long chains in solvent formed by short chains 10%.<sup>[29]</sup> The rise in the ratio of boric acid to hydroxyl-terminated PDMS results in increased relaxation time and  $G'$  at the elastic plateau (Figure S4, Supporting Information).

Visual appearance of blends. We observed that carbon volume fraction strongly affects the appearance and mechanical properties of blends (Figure 1). Blends with a low fraction of carbon

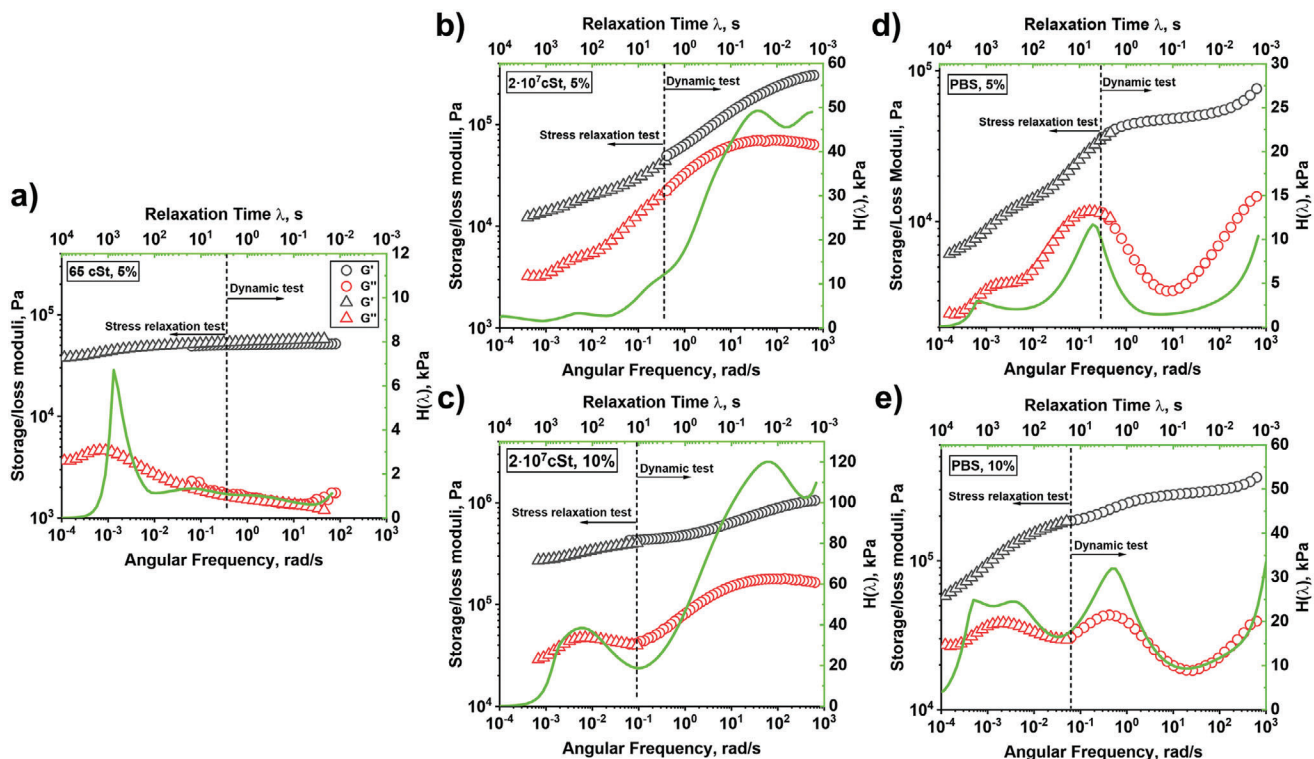


**Figure 2.** Viscoelastic behavior of PDMS-carbon blends at small deformation: a) PDMS 65 cSt 5% CB; PDMS  $2 \times 10^7$  cSt b) 5% CB and c) 10% CB; PBS d) 5% CB and e) 10% CB. Storage and loss moduli were obtained from both relaxation and dynamic experiments demonstrating viscoelastic behavior ranging from around  $10^{-4}$  to  $10^3$  rad  $s^{-1}$ . The relaxation spectra were calculated from merged experiments demonstrate the polymer and carbon black particle network's relaxation processes.

nanoparticles (5–10%) behave as dough. Nanoparticles are meanwhile barely observable on the surface of the polymer. An increase in the fraction of nanoparticles makes them visible on the surface. At CB content larger than 10 vol%, the composites become brittle and start behaving as a wet sand rather than as dough-like material. Thus, composites with 5 and 10 vol% of CB were chosen for further experiments

## 2.2. Viscoelastic Behavior of Blends at Small Deformations

Next, we studied the viscoelastic behavior of blends at small deformation, which does not introduce structural changes in materials (linear viscoelastic regime,  $\epsilon = 0.05\%$ ). Frequency sweep experiment performed in the range  $10^{-2}$ – $10^2$  Hz shows that for blends of PDMS 65 cSt with 5% and 10%, both storage and loss moduli increase with the rise of carbon content (Figures S2, S3, and S5, Supporting Information). The blends behave as elastic materials over the whole studied frequency range ( $G' > G''$ ) and moduli are nearly independent of frequency. It means that the materials are stable and do not flow on studied time scale at small deformation, i.e., small stress. Viscoelastic properties of blends of carbon with PDMS  $2 \times 10^7$  cSt and PBS are more complex. We observed the relaxation process on a time scale close to the relaxation time of corresponding polymers. This effect becomes less pronounced with the growth in carbon content. The transition to terminal flow regime was not observed within studied frequency

range, and  $G'$  is always larger than  $G''$  as well, confirming the stability of material at small deformation. Thus, it is notable that the addition of carbon nanoparticles to polymers renders its elastic properties—even blends of PDMS 65 cSt, which is Newtonian liquid, start to behave as pure elastic materials. The observed rheological behavior of blends of PDMS  $2 \times 10^7$  cSt and PBS with carbon show that it is a combination of viscoelastic properties provided by particles, similar to ones exhibited by PDMS 65 cSt blends, viscoelastic properties of long polymer chains and their interaction.

A relatively narrow probed time-scale range does not allow understanding of the whole picture of the viscoelastic behavior of the blends. Therefore, we combined frequency sweep and stress relaxation experiment to cover a broad time scale range in the range  $10^{-2}$ – $10^4$  s (Figure 2; and Figure S7, Supporting Information). The obtained results have been used for reconstruction of the dependence of  $G'$  and  $G''$  on the frequency and relaxation spectra according to Equations (3)–(6). It is important that all blends do not demonstrate transition to terminal flow regime even on the largest time scale and  $G'$  is always larger than  $G''$ . Relaxation time spectra of blends with the shortest PDMS (65 cSt) show a single weak peak at large time and nearly no relaxation of stress. The spectra of blends with long PDMS ( $2 \times 10^7$  cSt) chains and PBS contain two peaks: one at a short time scale ( $10^{-2}$ – $10^1$  s) and one at a large time scale ( $10^2$ – $10^3$  s). The position of the first peak nearly does not change with the increase in particle content (Figure 2). This peak can be

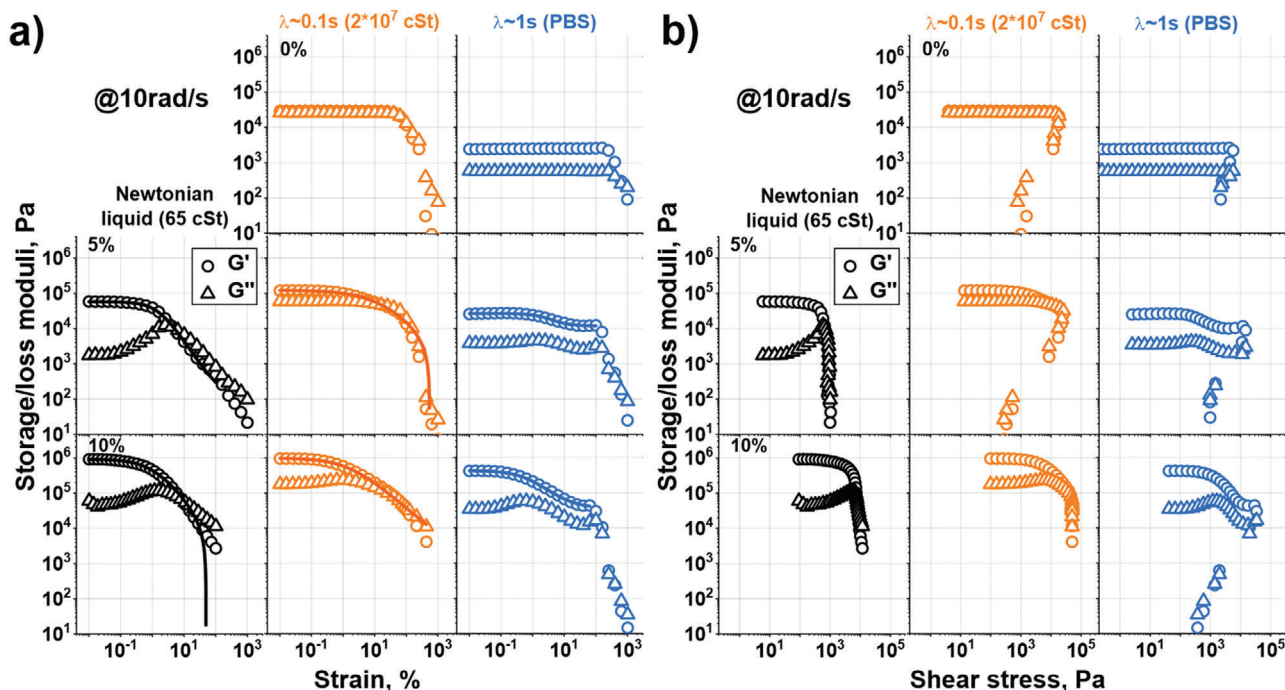


**Figure 3.** Amplitude sweep (at frequency  $10 \text{ rad s}^{-1}$ ) results of the pure polymers and their composites with 5 and 10 vol% of CB with  $G'$  and  $G''$  dependency on both a) shear strain and b) shear stress applied to a material.

attributed to the relaxation of polymer chains. The intensity of peak on large time increases with the increase of carbon content meaning that is associated with the movement of the particles. We calculated the time needed for the individual particles to move to the distance of their own size (average the square root of the mean square of displacement is  $\approx 50 \text{ nm}$ ), which is expected to correlate with relaxation time, to be in range  $\approx 10^3 \text{ s}$  (Figure S6, Supporting Information). This time scale correlates with time scale of the relaxation peak of the particles in high viscous PDMS  $2 \times 10^7 \text{ cSt}$  and PBS matrixes. However, relaxation in low viscous PDMS  $65 \text{ cSt}$  is observed on a much larger time scale than that corresponding to movement of the individual particles. The process occurring on this time scale in this polymer can be attributed either to the relaxation of small individual aggregates of particles or/and elements of carbon particles network. The weakness of this peak indicates that number of relaxing elements (individual aggregates of particles or elements of carbon particles network) is small. Thus, the addition of particles results in considerable change of viscoelastic behavior of polymers at small deformation—particles introduce elastic behavior on time scale at least up to  $10^4 \text{ s}$  (2 h), meaning that polymer–particle blends are not able to spread if applied force is small. There is, however, a difference between the behavior of blends with low molecular weight PDMS, high molecular weight PDMS and PBS—the higher is the relaxation time of the polymer matrix, the more pronounced is the drop of moduli on the larger time scale and the lower is the value of stress at large time scale: 40 kPa for 65 cSt, 10 kPa for  $2 \times 10^7 \text{ cSt}$ , and 6 kPa for PBS at 5 vol% of CB. This means that the quality of the particle network degrades with an increasing relaxation time of the polymer matrix.

### 2.3. Viscoelastic Properties at Large Deformations

It is essential to investigate behavior of the composites at different amplitudes of deformations to understand limits of their applicability. We applied amplitude sweep at  $10 \text{ rad s}^{-1}$  corresponding to time  $t = 0.1 \text{ s}$ , which is larger than relaxation time of PDMS  $65 \text{ cSt}$ , nearly corresponds to the relaxation time of PDMS  $2 \times 10^7 \text{ cSt}$  and less than the relaxation time of PBS. The results are plotted as dependence of  $G'$  and  $G''$  versus amplitude and versus stress (Figure 3; and Figures S9–S12, Supporting Information). Pure PDMS  $65 \text{ cSt}$  is Newtonian liquid, and its viscosity is independent of strain amplitude. Both  $G'$  and  $G''$  of PDMS  $2 \times 10^7 \text{ cSt}$  are nearly independent of amplitude and applied stress at small and moderate deformations. Both moduli decay—material fails at large deformations  $\approx 52\%$  and stress 16 kPa.  $G'$  and  $G''$  of PBS are constant over the amplitude range up to 206% and stress  $\approx 5 \text{ kPa}$  (Figure S8, Supporting Information).

The addition of particles changes rheological behavior. PMDS  $65 \text{ cSt}$  blends, as it was also discussed above, has elastic behavior at small deformation ( $G' > G''$ ). Increase in amplitude to  $\approx 0.1\%$  results in deviations from the linear regime, then  $G''$  goes over a maximum followed by domination of  $G''$  over  $G'$ , where gel–sol transition occurs (quantitative data are presented in the Table 1). The stress, at which deviations from the linear regime and domination of  $G''$  over  $G'$  increases with the fraction of particles. Thus, blends of Newtonian liquid and particle behave here as plastic materials—moduli drop at tiny deformations due to cohesion failure (Figure S14, Supporting Information). The stress becomes independent of deformation, meaning that contacts between particles do not break irreversibly but restore.

**Table 1.** Amplitude sweep data for shear strain and stress at  $G''$  and sol–gel transition/breakage points for polymers blends with various CB content.

Polymer matrix	vol% of CB	Elongation at max $G''$ [%]	Stress at max $G''$ [kPa]	Elongation at $G'' = G'$ [%]	Stress at $G'' = G'$ [kPa]
65 cSt	5	1.5	0.6	5.1	0.7
	10	0.9	5.8	9.4	7.7
$2 \times 10^7$ cSt	0	—	—	52	16
	5	—	—	21	13
	10	1.3	6	49	48
PBS	0	—	—	206	5
	5	1.8	0.2	130	13
	10	0.8	1.6	82	32

Properties of PDMS  $2 \times 10^7$  cSt are also affected by the presence of the carbon. As discussed above, PDMS  $2 \times 10^7$  cSt blends have elastic behavior at small deformation:  $G' > G''$ . Rise of amplitude to 0.1% results in deviations from the linear regime. No maximum of  $G''$  was observed at a low concentration of carbon that is most probably due to the domination of mechanic properties of PDMS: PDMS  $2 \times 10^7$  has a much higher elastic modulus than particle network does. Similar to PDMS 65 cSt blend, maximum for 10% of carbon in blend with PDMS  $2 \times 10^7$  cSt was observed at  $\epsilon = 1.3\%$ . However, the further increase in amplitude does not result in  $G''$  dominating  $G'$  and only at  $\epsilon = 21\%$  and 49% for 5 and 10 vol% of carbon, respectively, at which pure polymer fails,  $G''$  becomes larger than  $G'$ . The failure has a different character depending on the fraction of particles: 5% blend fail with drop of stress upon increase of strain, which is usual behavior of pure polymer; 10% blend shows plastic behavior that is similar to that of blends of low molecular weight PDMS (65 cSt) and stress is independent of deformation above flow point. This observation can be explained by the assumption that polymer determines failure at low particle content, and particles determine failure at their high content.

Blends of PBS with carbon particles behave as elastomer-particle blends described by Payne<sup>[30]</sup>— $G'$  is constant at small deformation, an increase of amplitude results in its gradual decrease, accompanied by a pronounced peak of  $G''$ , and then it again becomes constant. Similar to the previous two cases, an increase of amplitude to  $\approx 0.1\%$  results in deviations from the linear regime. Then  $G''$  goes over a maximum with a decrease in storage modulus, but the material still maintains its elastic properties. The drop of  $G'$  at large amplitude increases with the growth of particle content, although it does not reach the value of  $G'$  of pure polymer observed at large amplitude. The materials undergo failure at higher amplitude  $\epsilon \geq 130\%$  and  $\epsilon \geq 82\%$  for 5 and 10 vol% of carbon, respectively, which is quite close to the strain value for pure polymer, but still lower—stress drops with the increase of strain. One can say that particles determine viscoelastic properties at low amplitude and polymer determine at high amplitude. The polymer also determines the failure. Thus, an increase of relaxation time of polymer matrix results in a decrease in the influence of particles on failure.

Apparently, the relation between the relaxation time of matrix and time scale of deformation determines properties of viscoelastic blends not only at small but also at large deformations: either they are plastic or elastic. We tested this hypothesis by making

an amplitude test at various frequencies: 0.02 and 10 rad  $s^{-1}$  (Figure 4), at which PBS undergoes terminal flow and is elastic, respectively. The same experiments were conducted with PDMS 65cSt blends as reference material (Figure 4a; and Figure S15, Supporting Information). We observed nearly no effect of deformation rate of the behavior of PDMS 65 cSt blends—all of them are elastic before yield point and plastic after yield point independently of deformation rate.

Contrary to the behavior PDMS 65 cSt blends, the behavior of PBS is strongly affected by deformation rate. The blend is elastic at small deformation amplitude at low frequency when carbon network exists, and polymer matrix undergoes flow (0.02 rad  $s^{-1}$ ), and it flows at large deformation amplitude at low frequency. Contrary to PDMS 65 cSt blend, which shows plastic behavior of particle dispersion—stress is independent of amplitude above yield point (modulus drops at constant stress), PBS blends show flow behavior of polymer solution—loss modulus dominates, and it comes to the plateau with the increase in the amplitude. The same transition from particle flow behavior to polymer flow is observed in 5% of CB blends upon the increase of molecular weight of PDMS (Figures S9 and S10, Supporting Information). At high frequency, the PBS blend behaves as rubber with a filler—an increase in amplitude results in a break of particle agglomerates and elastic modulus decrease. The deformation, at which deviation from linear viscoelastic behavior and maximum of  $G''$  were observed at  $\approx 0.1\%$  and  $\approx 1.8\%$ , respectively, for 5 vol% of CB and  $\approx 0.1\%$  and  $\approx 0.8\%$  for 10 vol% of CB, and are independent of deformation rate. Thus, one can say that both polymer and particles determine nearly pure elastic behavior at high frequency at low amplitude, mostly polymer determines nearly pure elastic behavior at high frequency at high amplitude, particles determine nearly pure elastic behavior at low frequency at low amplitude and mostly polymer determines viscous flow behavior at low frequency at high amplitude (Table S3 and Figure S16, Supporting Information). Important, storage moduli of PBS 5% and 10% blends at low frequency (when polymer flows) and at low amplitude are lower than storage of PDMS 65 cSt blends with the same fraction of carbon, indicating the lower density of particle network in the case of PBS blend for the same CB volume fraction.

Increase in the fraction of carbon in blend with PBS results in the change of the character of the dependence of moduli on amplitude (Figure 4, PBS 10% CB). First,  $G'$  and  $G''$  become less dependent on frequency at low amplitude that is qualitatively

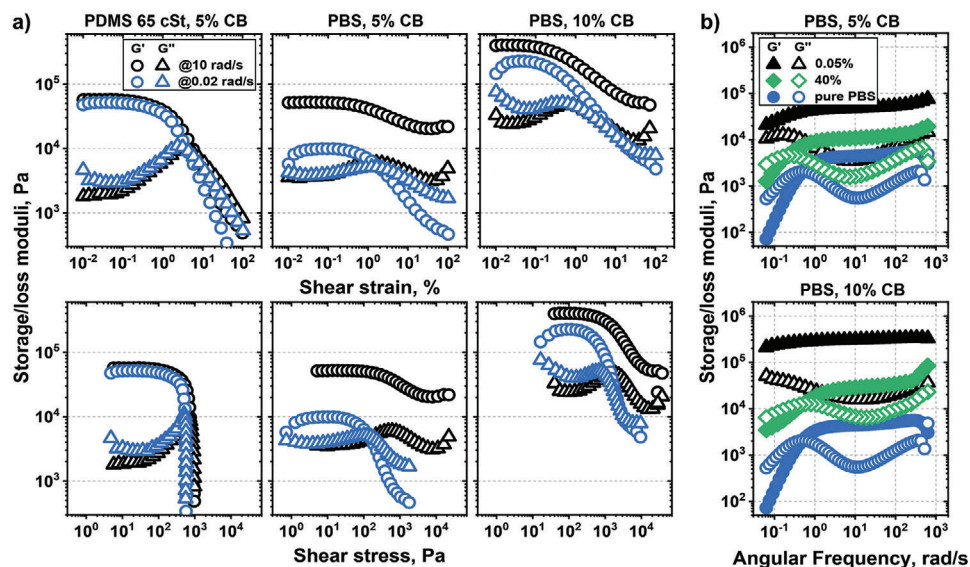


**Figure 4.** Viscoelastic behavior of polymer-carbon blends at large amplitude: a) amplitude sweep results, performed at various frequencies, of composites of PDMS 65 cSt as Newtonian liquid and PBS with relaxation time  $\lambda \approx 1$  s with 5 and 10 vol% of CB where  $G'$  and  $G''$  dependency is on both shear strain and shear stress applied to a material. b) The frequency sweep test of PBS with 5 and 10 vol% of CB at 0.05% and 40% of shear strain corresponding to first and second linear region of the materials, respectively.

similar to behavior of PDMS 65 cSt blend. Second,  $G'$  and  $G''$  drop sharper and at higher stress that is similar to behavior of carbon-PDMS 65 cSt blend. These two effects originate from increasing particle contribution to mechanical properties. On the other hand,  $G''$  dominates over  $G'$  at high-stress, and come to a plateau corresponding to behavior of polymer that is qualitatively similar to sample with 5% carbon—10% PBS blend flows as particle-filled polymer dispersion at large amplitude and stress.

In order to obtain the whole picture of viscoelastic behavior of blends at different amplitudes and frequencies, we made frequency sweep experiment at low strain ( $\epsilon = 0.05\%$ , particle network exists) and large strain ( $\epsilon = 40\%$ , particle network of carbon is broken) (Figure 4b). Decrease of angular frequency results in relaxation of polymer chains and decrease of moduli, which becomes pronounced at large amplitude of deformation. Both PBS 5% and 10% blends show the drop of  $G'$  in the rubbery plateau region upon increase of amplitude, and the drop increases with carbon fraction. However, value of  $G'$  of composites in rubbery plateau region at large amplitude of deformation is still higher than that of pristine PBS. The essential difference between small- and large-amplitude frequency sweep is observed at the time scale above the relaxation time of polymer. Both PBS 5% and 10% composites are elastic ( $G' > G''$ ) at low amplitude of deformation and flow at large amplitude at low frequency with cross-section point at a frequency slightly lower than that of pristine PBS (Figure 2) that is due to lower mobility of partially adsorbed on particles polymer chains. Thus, the material rheological properties with lower carbon content at large shear strain are determined mostly by polymer matrix since gel network is broken and carbon particles play reinforcing function due to direct interaction with polymer chains only. On the other hand, it is challenging to disregard the CB network entirely with higher filler content, which explains the brittleness of materials.

#### 2.4. Creep Experiment

We performed creep experiment by applying stress below the value at which particle-particle contact breaks and above with 5% of CB blends and different matrices (Figure S17, Supporting Information). It was found that applying low stress results in negligible creep—viscosity is in the range of 0.1–10 GPa s. Notably, blend with PBS creeps better (viscosity is lower) than ones with PDMS 65 cSt that is an indication on defects in the network or worse contact between particles. Applying large stress results in cohesion failure (Figure S14, Supporting Information) in the case of PDMS 65 cSt—the rheometer plate starts to rotate very quickly. The viscosity of PDMS  $2 \times 10^7$  cSt and PBS blends drop down to  $\approx 210$  and 79 kPa s, respectively. At this force, the carbon network is broken; meanwhile, the polymer matrix maintains material integrity and provides its flow. Thus, the creep experiment indicates defects in the particles network in PBS blends.

#### 2.5. Steady State Rheology

The rotational experiment was performed to understand spreading (flow) properties of blends (Figure 5). Pure PDMS 65 cSt behaves as a Newtonian liquid, and its viscosity is rate-independent. The viscosity of PDMS  $2 \times 10^7$  cSt and PBS is also independent of rate when the rate is below reciprocal relaxation time ( $1/\lambda$ ) because materials are in a terminal flow regime. The viscosity of PBS slightly increases upon approach to the rate corresponding to relaxation time. It then rapidly drops in the way that stress decreases with further increase of rate—materials undergo failure. Apparently, materials flow at low rates, at some point undergoes transition to elastic states, in which it breaks upon stretching. Similar behavior is observed in the case of PDMS  $2 \times 10^7$  cSt—viscosity is independent of rotation rate polymer fails at time scale close to relaxation time.

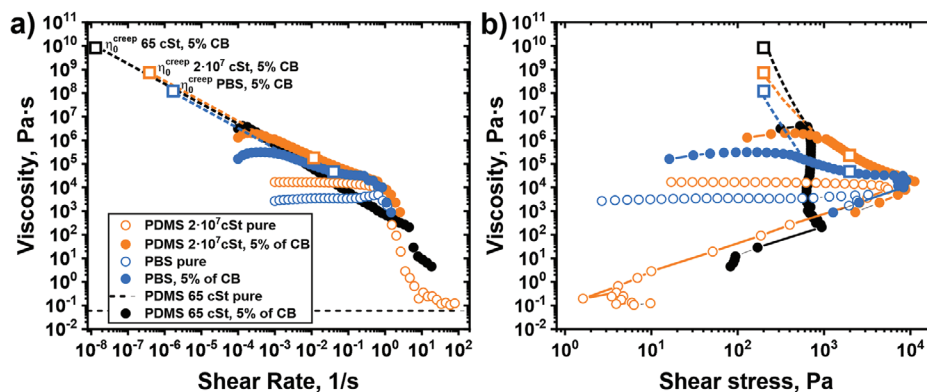


**Figure 5.** Rotational test results of the pure polymers and their composites with 5 vol% of CB with viscosity dependency on both a) shear rate and b) shear stress applied to a material. Empty squares are results of creep experiment. Dashed lines show expected evolution of viscosity with rate and stress when steady state flow at low shear rates will be achieved.

The addition of filler particles increases the viscosity of materials. It becomes strongly dependent on the rate of rotation – the blends demonstrate a pronounced decrease in viscosity with increase of rate—shear thinning behavior. The character of the decrease depends on viscoelastic behavior of polymer matrix. In the case of PDMS 65 cSt, viscosity drops rapidly upon the increase in shear rate as soon as applied stress is  $> 600$  Pa, and an increase in rotation rate does not increase stress. Such behavior can be attributed to cohesion failure. Further increase of rotation rate (above  $50 \text{ s}^{-1}$ ) results in rapid drop of stress—material comes out from the space between rotating plates. Blends of PDMS  $2 \times 10^7$  cSt and PBS demonstrate classical shear thinning behavior—viscosity drops at certain value of stress ( $\approx 300\text{--}400$  Pa) that is due to failure of contacts between particles. Viscosity remains constant for PBS blend with further increase in rotation rate and applied stress because the polymer is terminal flow regime and contribution of particles to viscosity is low because contacts between them are broken. Similar to pure polymer, an increase in rotation rate to the value corresponding to the relaxation time of polymer results in its transition to elastic state, and polymer fails—both stress and viscosity drop rapidly. It is also worth noting that the highest Newtonian viscosity of the blends obtained by steady state measurement is not reliable since for each point the measurement time should be at least  $1/\dot{\gamma}$  s (the materials does not achieve a plateau at low shear rate). Therefore, the viscosity values are more credible from much longer creep experiment (square points on the plot). Thus, steady-state rheology revealed three distinct flow regimes of polymer–particle blends with viscoelastic polymer matrix: i) high viscosity regime at low stress when particle–particle contacts exist; ii) shear thinning and transition to polymer flow, and iii) polymer failure.

## 2.6. Electrical Characterization

According to the literature, all investigated polymer–particle blends lie behind the percolation threshold, which is around 0.25 vol% for linear low viscous PDMSs<sup>[31]</sup> and 1.25 vol% for PBS-like Silly Putty.<sup>[32]</sup> Therefore, we investigated the character of electric resistivity (real/imaginary) of polymer–carbon blends to understand the nature of structures formed by particles. We first an-

alyzed the current–voltage behavior of materials (scanning rate is  $100 \text{ V s}^{-1}$ ). There are two distinct regimes: low conductivity at low ( $-1 \div 1 \text{ V}$ ) voltage and higher conductivity at high ( $V > 2 \text{ V}$ ,  $V < -2 \text{ V}$ ) voltage (Figure 6a,b; and Figure S18, Supporting Information). The voltage range of low conductivity regime apparently decreases with increase of carbon content. To understand effects of relaxation properties of polymer and amount of particles on electrical properties of composite, we tested the electrical conductivity properties of the materials by electrochemical impedance spectroscopy (EIS) at different offset voltages and amplitudes of oscillations that covers low- and high-conductivity regimes.

It was found that frequency range, at which impedance is mostly real, decreases with the increase of relaxation time (and molecular weight) of polymer in low conductivity regime (small voltage amplitude (10 mV and 0 V offset) (Figures S19–S21 and 23a,b, Supporting Information). Bode plots also show that increase of relaxation time results in appearance of two relaxation transitions that can also be seen in the Nyquist plots (Figure 6c)—carbon blends of PDMS  $2 \times 10^7$  cSt and PBS show two semicircles, while the Nyquist plot for the 65 cSt 5% composite has one semicircle. We fitted the Nyquist plot according to the equivalent scheme of the impedance spectra shown in Figure 6c, which consists of resistor  $R_0$  in series with two RC-elements of resistor  $R_i$  and capacitor  $C_i$ , connected in parallel. As fitting algorithm, the Levenberg–Marquardt method was used. The fitting parameters are summarized in Table 2, where  $R_0$  can be attributed to the resistivity of measuring system contacts and bulk conductivity of CB network between direct contacts of the particles, and  $R_1$ ,  $C_1$ ,  $R_2$ ,  $C_2$  to materials parameters. We speculate that the resistivity  $R_1$  and  $R_2$  can be attributed to tunneling (hopping) conductivity across small gaps ( $< 10 \text{ nm}$ ) between CB particles aggregates, which is typically observed in CB–polymer composites.<sup>[33,34]</sup> Particles that are close to each other but do not form contacts form a pseudocapacitor on interface. The EIS results may also be described by a finite number of RC elements, spread over a wider range of time constants, since the distance between the aggregates is nonuniform. It can then be presented as a distribution of relaxation times function<sup>[35–37]</sup> (Figures S19b and S22, Supporting Information). However, for our evaluation, we have only taken two such elements for an average estimate of this conductivity contribution

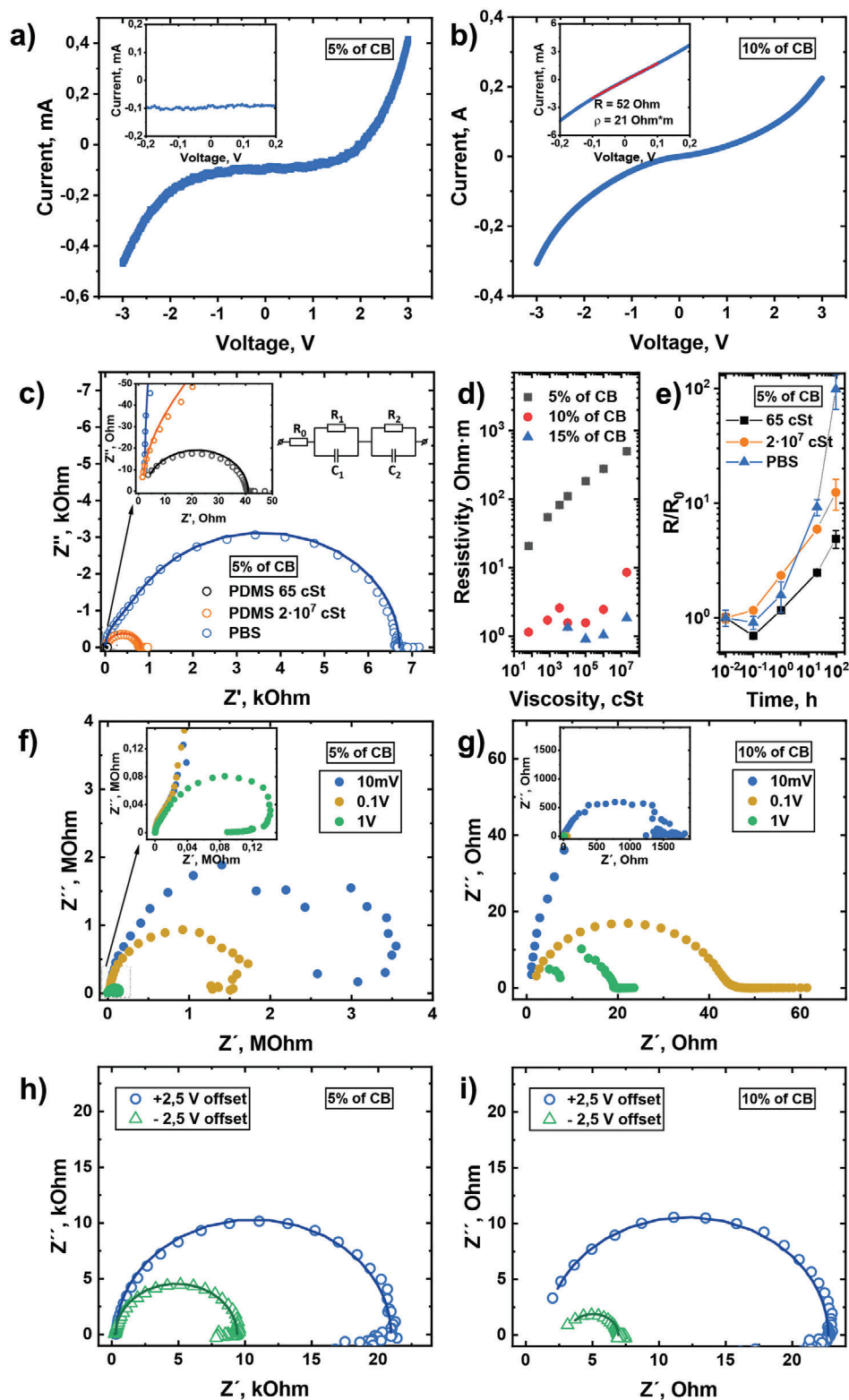


**Figure 6.** a) Volt-ampere characteristic of PBS–CB blends in voltage range  $-3 \text{ V} < V < +3 \text{ V}$  measured at  $100 \text{ mV s}^{-1}$  scanning rate. c) Nyquist plot of EIS of a polymer–CB composites at 0 V offset with 10 mV amplitude fitted according to equivalent electrical circuit by Levenberg–Marquardt method of optimization. d) Resistivity dependence of composites of different molecular weight linear PDMS with various CB content. e) Resistivity change of CB–polymer composites with 5% of CB with time at rest. f,g) Nyquist plot of EIS of a PBS–CB composites at 0 V offset with 2.5 V amplitude. h,i) Nyquist plot of EIS of a PBS–CB composites at 2.5 V offset with 10 mV amplitude fitted by Levenberg–Marquardt method with the same equivalent circuit.

**Table 2.** Fitting parameters of EIS data for polymers composites with 5 vol% of CB at offset  $V = 0$  V, amplitude 10 mV (Figure 6c) and for PBS composites with 5 and 10 vol% of CB at offset  $V = \pm 2.5$  V, amplitude 10 mV data (Figure 6h,i).

	Offset [V]	$R_0$ [Ohm]	$R_1$ [Ohm]	$C_1$ [nF]	$R_2$ [Ohm]	$C_2$ [nF]
65 cSt, 5%	0	2.7	—	—	38	19
$2 \times 10^7$ cSt, 5%	0	1.5	766	41	38	43
PBS 5%	0	2.3	6151	28	557	29
PBS 5%	2.5	202	20 640	17	117	2.6
	-2.5	196	9112	19	92	6
PBS 10%	2.5	1.5	19	41	2.3	331
	-2.5	3.2	2.4	162	1.4	286

Character of evolution of conductivity of polymer-carbon blends with relaxation time of polymers depends on fraction of carbon (Figure 6d). For linear PDMSs blends, we observed that the resistivity at low frequency ( $R_0 + R_1 + R_2$ ) increases with the increase in viscosity (molecular weight, relaxation time) at low carbon content (5%) (Figure S23, Supporting Information) and is nearly independent on viscosity at higher carbon content >10%. The highest resistivity is observed for PBS composites. This observation is in accordance with rheological data, which indicate that quality of particle network becomes worse with the increase of molecular weight and relaxation time of polymer.

Important, resistivity of polymer-carbon blends changes with time, and the character depends on relaxation time of polymer matrix (Figure 6e). While the resistivity of PDMS 65 cSt-carbon blends increases fourfold (nearly a half an order of magnitude) on time scale of 100 h, resistivity of PBS-carbon blend increases by 100 times—two orders of magnitude. These changes in resistivity indicate on worsening of quality of carbon network with time.

Increase in the amplitude of voltage oscillation results in the decrease of the impedance as it could also be expected from character of  $V-I$  dependence—a transition from low conductivity regime to high conductivity regime shall be observed (Figure 6f,g; and Figure S24, Supporting Information). The character of decrease of impedance depends on fraction of carbon. An increase in amplitude from 10 to 100 mV results in considerable decrease of electrical impedance at 10%, while impedance at 5% decreases relatively weak. Further increase of amplitude to 1 V results in significant decrease of impedance at 5% of carbon, while impedance at 10% decreases relatively weakly. This means that the voltage range, at which low conductivity regime is observed becomes narrower with increasing carbon content.

Next, we measured electrical impedance in high conductivity regime by applying low amplitude oscillations (10 mV) at positive and negative at offset voltages ( $V_0 \pm 2.5$  V) (Figure 6h-i; and Figure S25, Supporting Information). The Nyquist plot of EIS results shows only one semicircle, which we attribute to the tunneling conductivity of materials. The tunneling current ceases to dominate at these voltage values,<sup>[38]</sup> and electrical breakdowns between separated CB particles and aggregates occur. Therefore, for the application of the composite, where high conductivity is required, a voltage higher than  $\approx 2$  V should be used to prevent the impact of nonlinear tunneling current.

Thus, conductivity measurements allow making conclusions about structure of polymer-particle blends. The low conductivity at 0 V offset with low voltage amplitude is due to absence of direct contacts between the particles—they are most probably separated by polymer chains. Hopping conductivity at small voltage barely occurs and material possess high resistivity. The particles are, however, close to each other, and by applying higher voltages, “electrical breakdown” is observed that increases conductivity. The higher the fraction of particles and the lower the molecular weight and relaxation time of insulating polymer are, the more direct contacts between the particles and the closer are the particles, which do not have direct contact with each other. As a consequence, stronger filler network forms and material possesses higher conductivity.

## 2.7. Self-Healing Behavior

Finally, we studied the self-healing behavior—recovery of electrical and mechanical properties of the blends after mechanical shear deformation at different amplitudes. The time-sweep measurements of impedance (at 50 Hz at offset voltage 0 V), and storage/loss moduli (at shear stress 0.01% and frequency 1 rad s<sup>-1</sup>) were carried out simultaneously after a sequence of several one-step shear strains followed by materials restoration (Figure 7; and Figures S26–S28, Supporting Information). We selected several amplitudes, which correspond to different structural transitions in materials. The 1% of shear strain related to pseudolinear viscoelastic region (before  $\epsilon_c$ ), 10% corresponds to nonlinear region, where agglomerates network undergoes breakage, and 1000% corresponds to material failure. At  $\epsilon = 1\%$ , the storage modulus of PDMS 65 cSt with 5% of CB changes negligibly. The loss modulus rapidly increases and then decreases back to the initial value within experiment time. The energy dissipates due to the friction between particles, however, the agglomerates network is not broken yet. Resistivity qualitatively follows behavior of  $G''$ —it increases upon deformation and then decreases to initial value. Applying of large deformations (10% and 1000%) results is a drop of storage modulus due to the destruction of the carbon grid in the polymer matrix. As soon as the deformation is removed,  $G'$  immediately restores. The restoration of  $G''$  and resistivity at large deformations (10% and 1000%) is similar to that after 1% deformation.

Blends of carbon with PDMS  $2 \times 10^7$ cSt and PBS behaves differently than PDMS 65 cSt-carbon blend. At small deformation (1% and 10%), the storage modulus drops and then restores, while loss modulus remains nearly unchanged—elastic behavior of polymer dominates at the conditions of rheological experiment and contribution of particles is not visible. Increase of amplitude to 1000% (failure of polymer) results in drop of both storage and loss moduli, and they increase upon recovery. Important, the recovery of moduli after deformation of PDMS  $2 \times 10^7$  cSt and PBS-carbon blends is much slower than of PDMS 65 cSt-carbon blend (Figure S28, Supporting Information). That is due to high viscosity of polymer, which slows down restoration of carbon network—evidence of thixotropic behavior. In the case of these two polymers, resistivity was not able to reach its initial value before. Moreover, deviation of value of resistivity after recovery from that before mechanical stimula-

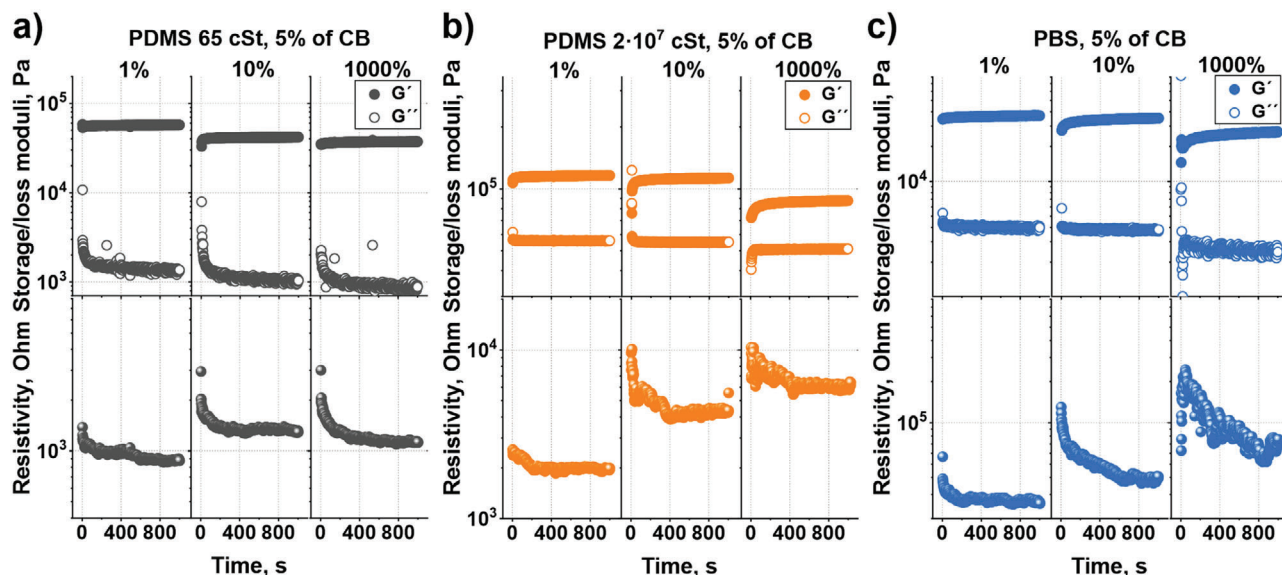


**Figure 7.** Time-sweep measurements of resistivity and storage/loss moduli of 5% CB-polymer composites with a) PDMS 65 cSt, b) PDMS  $2 \times 10^7$  cSt, and c) PBS as polymer matrix after one-step shear strain varying from 0.05% and 1000% followed by moduli measurements at small strain (0.01%) and frequency (1 Hz).

tion is larger in the case of PDMS  $2 \times 10^7$  cSt blend that is due to its higher viscosity comparing to that of PBS. Thus, the recovery of the mechanical and conductive properties of blends of viscoelastic polymers with CB worsens with increasing polymer viscosity, rather than with increasing polymer relaxation time.

### 3. Discussion

We performed a thorough characterization of rheological, mechanical, and electrical properties of self-healing PBS-carbon blends and reference carbon blends with low and high molecular weight PDMS. There are several indications that the quality of particle network in PBS-carbon blends is worse than that in blends of carbon with low molecular weight PDMS. There are individual particles, large individual agglomerates, and dangling agglomerates in PBS-carbon blends that is evidenced by i) polymer-like character failure PBS-carbon blend, ii) low modulus at frequency below relaxation time of polymer, iii) relaxation peak corresponding to individual particles; iv) more pronounced creep at stress below yield point, v) lower conductivity, and it decreases with time—network break down by itself, and vi) slow restoration of mechanical properties and conductivity after failure. The reason for formation of poor carbon network in PBS-carbon blends is apparently the adsorption of polymer chains on particles via weak Van der Waals interaction, forming a special interfacial insulating shell with thickness  $t$ , properties of which differ from bulk polymer. For linear polymers, the  $t$  can be accepted as half of the gyration radius, which is 0.25 and 1.94 nm for PDMS 65 cSt and  $2 \times 10^7$  cSt, respectively. For elastomers, this value is about 10 nm. The larger the interfacial volume, the more substantial entropy impact, which leads to better dispersion of CB in polymer matrix overcoming enthalpy of CB particle-particle attraction. Consequently, the composites of Newtonian

liquid PDMS 65 cSt with the lowest interfacial volume, where polymer-particles interaction is due to capillary forces only, form a strong agglomeration network. Apparently, the formation of polymer shell around particles occurs not immediately. It is a slow process as can be concluded from rate of increase of resistivity with time. The structure of low and high molecular weight polymer-carbon blends is schematically depicted in Figure 8.

### 4. Conclusions

We performed a thorough study of electromechanical and rheological properties of blends of carbon particles and PDMS with different relaxation times. Adding carbon filler to the polymers renders its new properties, and behavior of composites depends strongly on the viscoelastic properties of polymers. The polyborosiloxane allows the dough-like behavior of the blends. The material possesses elastomer-like behavior on a small time scale. It flows on a large time scale when large stress is applied and can withstand large deformation without brittle failure. On the other hand, the viscoelastic self-healing polymer negatively affects the stability of carbon-carbon contacts, which ensures high conductivity. As a result, the electrical properties of blends of viscoelastic polymers and carbon are worse than that of carbon and viscous polymer. Moreover, the viscoelastic polymer degrades the conductive carbon networks with time, decreasing its conductivity. Ability of polymer-carbon composites to flow, which is utilized for self-healing, is an indication of absence of 3D network formed by particles. It results in worse conductivity compared to the blends with low molecular weight polymer, which do not flow due to formation of carbon network, have brittle failure but is able to immediately restore mechanical properties and conductivity after removing stress.

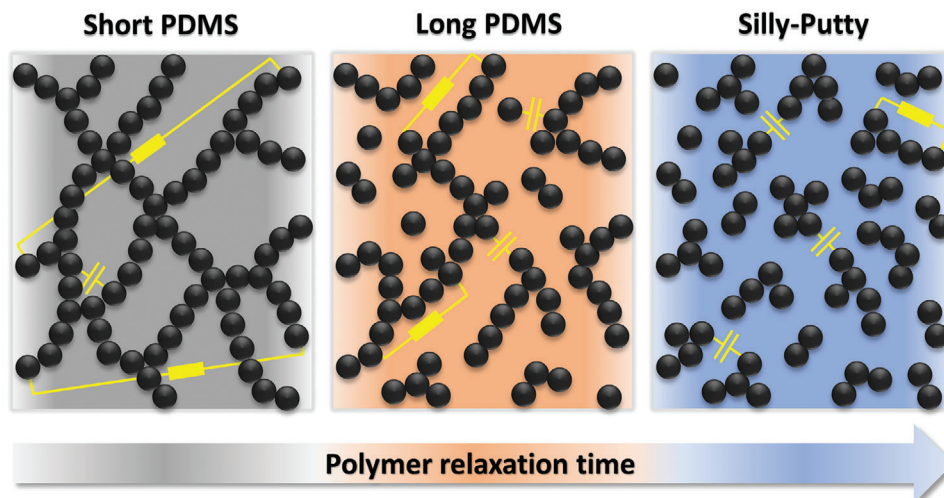


**Figure 8.** The scheme of agglomeration network of CB in polymer matrix with very low relaxation time (PDMS 65 cSt), PDMS  $2 \times 10^7$  cSt with relaxation time  $\approx 0.1$  s, and PBS with relaxation time  $\approx 1$  s. Pseudocapacitor and resistor elements of network are marked in yellow signs.

## 5. Experimental Section

**Materials:** The hydroxyl-terminated PDMS with kinematic viscosity 65 cSt, 750 cSt, and 3500 cSt and methyl-terminated PDMS with kinematic viscosity  $10^4$  cSt,  $10^5$  cSt,  $10^6$  cSt, and  $2 \times 10^7$  cSt were purchased from Sigma-Aldrich and Gelest company, respectively. The highest Newtonian viscosity was calculated using the value of specific gravity for each precursor. The number average molecular mass,  $M_n$ , and weight average molecular weight,  $M_w$ , and polydispersity index, PDI ( $PDI = M_w/M_n$ ), were determined by GPC (Agilent 1260 Infinity) (Figure S1b, Supporting Information). The measurements were carried out at 30 °C. The eluent for GPC measurements was tetrahydrofuran (THF) of high-performance liquid chromatography grade, and the standards used for calibration were monodisperse poly(methyl methacrylate). All obtained parameters are listed in Table S1 (Supporting Information). The plot  $\eta$  versus  $M_w$  for PDMS with kinematic viscosity from 3500 to  $2 \times 10^7$  cSt correlates with the typical power law  $\eta \approx M_w^{4.8}$  (Figure S1a, Supporting Information). The carbon black with BET determined surface area  $62 \text{ m}^2 \text{ g}^{-1}$  was purchased from Nanografi Company. Toluene ( $\geq 99.5\%$ ) and boric acid ( $\geq 99.5\%$ ) from Sigma-Aldrich, and Dichloromethane (DCM) (99.8%) from ACROS Organics were purchased and used as it is.

**PBS Synthesis:** To prepare PBS, the ratios between the hydroxyl-terminated PDMS 65 cSt and  $\text{H}_3\text{BO}_3$  100:0.85 (relaxation time is  $\approx 1$  s), 100:1.0 (relaxation time is  $\approx 10$  s), and 100:1.5 (relaxation time is  $\approx 100$  s) by mass were used. First, the PDMS was dissolved in toluene. Then, boric acid was added to the solution, and the mixture was dispersed for a couple of minutes in an ultrasonic bath. The mixture was heated to 120 °C and left for 24 h with further stirring. After this time, the mixture became transparent. Excess solvent was removed with a vacuum evaporator, and the rest of the solvent was removed by storing the sample in a vacuum oven at 60 °C for 24 h.

**Preparation of Polymer-CB Composites:** CB/PDMS and PBS/CB composites with various volume fractions of carbon material were synthesized, assuming that CB and polymers density are 2 and  $1 \text{ g cm}^{-3}$ , respectively. For composites with PDMS viscosity up to  $10^5$  cSt CB was added to PDMS solution in dichloromethane (DCM), which initially was taken in excess to permit easy mixing and dispersion of compounds. All compounds were preliminary dispersed in ultrasound bath and mixed with IKA RW 20 disperser for 30 min at 1200 rpm. Excess of DCM was evaporated in an ultrasonic bath and then in a vacuum desiccator for 30 min at 10 mbar and 20 °C. For composites with PDMSs with viscosity higher than  $10^6$  cSt and PBS, toluene as a solvent was used due to their low solubility in DCM. First, the polymer was dissolved in toluene at 60 °C in 1 h. Then, CB was added to polymer solution in toluene, and all compounds were first dis-

persed in ultrasound bath and then mixed with the same disperser for 30 min at 1200 rpm. Excess of toluene was evaporated in a vacuum desiccator. The rest of the solvent was removed by storing samples in a vacuum oven at  $T = 60$  °C for 24 h.

**Characterization:** The microstructure of composites was investigated by field emission scanning electron microscopy (FESEM) (Thermo Scientific, Germany). Rheological measurements were carried out with 25 mm parallel plate geometry on MCR 702 (Anton Paar, Graz, Austria) coupled with dielectric measuring cell. All samples were roughly flattened before lowering the rheometer to a gap size of  $\approx 1$  mm. Then samples were allowed to relax and reach measurement temperature for 15 min. EIS measurements were performed at 25 °C in frequency range from 0.1 Hz to 1 MHz on Gamry 1010E potentiostat.

The relaxation time  $\lambda$  is defined as the peak time of continuous relaxation spectra  $H(\lambda)$ , which is for infinite time-scale generalized Maxwell model can be expressed as

$$G'(\omega) - G_e = \int_{-\infty}^{\infty} H(\lambda) \frac{\omega^2 \lambda^2}{1 + \omega^2 \lambda^2} d(\ln \lambda) \quad (1)$$

$$G''(\omega) = \int_{-\infty}^{\infty} H(\lambda) \frac{\omega \lambda}{1 + \omega^2 \lambda^2} d(\ln \lambda) \quad (2)$$

The time-scale extension was achieved by relaxation experiment, where relaxation modulus was recalculated into relaxation spectra  $H(\lambda)$  and storage/loss moduli according to generalized Maxwell model as well<sup>[39]</sup>

$$G(t) = G_e + \sum_{i=1}^N g_i e^{-t/\lambda_i} \quad (3)$$

$$H(\lambda) = \sum_{i=1}^N g_i \delta(\lambda/\lambda_i - 1) \quad (4)$$

$$G'(\omega) = \omega \int_0^{\infty} G(t) \sin(\omega t) dt \quad (5)$$

$$G''(\omega) = \omega \int_0^{\infty} G(t) \cos(\omega t) dt \quad (6)$$

where coefficients  $g_i$ ,  $G_e$ , and relaxation times  $\lambda_i$  are material parameters,  $\delta(y)$  is the Dirac delta function.

## Supporting Information

Supporting Information is available from the Wiley Online Library or from the author.

## Acknowledgements

This work was supported by the DFG (Grant No IO 68/20-1, IO 68/21-1). Also, the authors would further like to thank Professor Scheibel for allowing the authors to use SEM equipment to conduct this research.

Open access funding enabled and organized by Projekt DEAL.

## Conflict of Interest

The authors declare no conflict of interest.

## Data Availability Statement

The data that support the findings of this study are available in the Supporting Information of this article.

## Keywords

carbon black, carbon-based materials, polyborosiloxane, polydimethylsiloxane, self-healing, self-healing electrodes, silly-putty

Received: March 30, 2022

Revised: April 22, 2022

Published online:

- [1] P. Tan, H. Wang, F. Xiao, X. Lu, W. Shang, X. Deng, H. Song, Z. Xu, J. Cao, T. Gan, B. Wang, X. Zhou, *Nat. Commun.* **2022**, *13*, 358.
- [2] J. Kang, J. B. H. Tok, Z. Bao, *Nat. Electron.* **2019**, *2*, 144.
- [3] E. Bozo, H. Ervasti, N. Halonen, S. H. H. Shokouh, J. Tolvanen, O. Pitkanen, T. Jarvinen, P. S. Palvolgyi, A. Szamosvolgyi, A. Sapi, Z. Konya, M. Zaccone, L. Montalbano, L. De Brauwier, R. Nair, V. Martinez-Nogues, L. San Vicente Laurent, T. Dietrich, L. Fernandez de Castro, K. Kordas, *ACS Appl. Mater. Interfaces* **2021**, *13*, 49301.
- [4] A. C. Marques, J.-M. Cabrera Marrero, C. de Fraga Malfatti, *Springer-Plus* **2013**, *2*, 521.
- [5] M. Kaltenbrunner, T. Sekitani, J. Reeder, T. Yokota, K. Kuribara, T. Tokuhara, M. Drack, R. Schwodiauer, I. Graz, S. Bauer-Gogonea, S. Bauer, T. Someya, *Nature* **2013**, *499*, 458.
- [6] Y. Zhang, C. K. Jeong, J. Wang, H. Sun, F. Li, G. Zhang, L.-Q. Chen, S. Zhang, W. Chen, Q. Wang, *Nano Energy* **2018**, *50*, 35.
- [7] K. Narumi, F. Qin, S. Liu, H.-Y. Cheng, J. Gu, Y. Kawahara, M. Islam, L. Yao in Proceedings of the 32nd Annual ACM Symposium on User Interface Software and Technology, 2019293, <https://dl.acm.org/doi/pdf/10.1145/3332165.3347901>.
- [8] N. De Belie, E. Gruyaert, A. Al-Tabbaa, P. Antonaci, C. Baera, D. Bajare, A. Darquennes, R. Davies, L. Ferrara, T. Jefferson, C. Litina, B. Miljevic, A. Otlewska, J. Ranogajec, M. Roig-Flores, K. Paine, P. Lukowski, P. Serna, J.-M. Tulliani, S. Vucetic, J. Wang, H. M. Jonkers, *Adv. Mater. Interfaces* **2018**, *5*, 1800074.
- [9] S. M. Bleay, C. B. Loader, V. J. Hawyes, L. Humberstone, P. T. Curtis, *Composites, Part A* **2001**, *32*, 1767.
- [10] S. R. White, N. R. Sottos, P. H. Geubelle, J. S. Moore, M. R. Kessler, S. R. Sriram, E. N. Brown, S. Viswanathan, *Nature* **2001**, *409*, 794.
- [11] X. Luo, P. T. Mather, *ACS Macro Lett.* **2013**, *2*, 152.
- [12] J. C. Cremaldi, B. Bhushan, *Beilstein J. Nanotechnol.* **2018**, *9*, 907.
- [13] Y. Yang, M. W. Urban, *Chem. Soc. Rev.* **2013**, *42*, 7446.
- [14] Y. L. Rao, A. Chortos, R. Pfattner, F. Lissel, Y. C. Chiu, V. Feig, J. Xu, T. Kurosawa, X. Gu, C. Wang, M. He, J. W. Chung, Z. Bao, *J. Am. Chem. Soc.* **2016**, *138*, 6020.
- [15] F. Herbst, S. Seiffert, W. H. Binder, *Polym. Chem.* **2012**, *3*, 3084.
- [16] S. Burattini, B. W. Greenland, D. H. Merino, W. Weng, J. Seppala, H. M. Colquhoun, W. Hayes, M. E. Mackay, I. W. Hamley, S. J. Rowan, *J. Am. Chem. Soc.* **2010**, *132*, 12051.
- [17] A. Kurkin, V. Lipik, K. B. L. Tan, G. L. Seah, X. Zhang, A. I. Y. Tok, *Macromol. Mater. Eng.* **2021**, *306*, 2100360.
- [18] E. D'Elia, S. Barg, N. Ni, V. G. Rocha, E. Saiz, *Adv. Mater.* **2015**, *27*, 4788.
- [19] Z. Chang, Y. He, H. Deng, X. Li, S. Wu, Y. Qiao, P. Wang, H. Zhou, *Adv. Funct. Mater.* **2018**, *28*, 1804777.
- [20] Y. J. Tan, J. Wu, H. Li, B. C. K. Tee, *ACS Appl. Mater. Interfaces* **2018**, *10*, 15331.
- [21] H. Wang, B. Zhu, W. Jiang, Y. Yang, W. R. Leow, H. Wang, X. Chen, *Adv. Mater.* **2014**, *26*, 3638.
- [22] P. Qu, C. Lv, Y. Qi, L. Bai, J. Zheng, *ACS Appl. Mater. Interfaces* **2021**, *13*, 9043.
- [23] Y. Chen, X. Pu, M. Liu, S. Kuang, P. Zhang, Q. Hua, Z. Cong, W. Guo, W. Hu, Z. L. Wang, *ACS Nano* **2019**, *13*, 8936.
- [24] T. Wu, E. Gray, B. Chen, *J. Mater. Chem. C* **2018**, *6*, 6200.
- [25] C. S. Boland, *ACS Nano* **2019**, *13*, 13627.
- [26] L. Van Beek, B. Van Pul, *J. Appl. Polym. Sci.* **1962**, *6*, 651.
- [27] L. J. Fetters, D. J. Lohse, S. T. Milner, W. W. Graessley, *Macromolecules* **1999**, *32*, 6847.
- [28] M. Tang, W. Wang, D. Xu, Z. Wang, *Ind. Eng. Chem. Res.* **2016**, *55*, 12582.
- [29] R. H. C. Michael Rubinstein, *Polymer Physics*, Oxford University Press, Oxford **2003**.
- [30] A. R. Payne, R. E. Whittaker, *Rubber Chem. Technol.* **1971**, *44*, 440.
- [31] M. Kontopoulou, M. Kaufman, A. Docoslis, *Rheol. Acta* **2008**, *48*, 409.
- [32] C. S. Boland, U. Khan, G. Ryan, S. Barwich, R. Charifou, A. Harvey, C. Backes, Z. Li, M. S. Ferreira, M. E. Möbius, R. J. Young, J. N. Coleman, *Science* **2016**, *354*, 1257.
- [33] P. Sheng, E. K. Sichel, J. I. Gittleman, *Phys. Rev. Lett.* **1978**, *40*, 1197.
- [34] A. Narayanan, F. Mugele, M. H. Duits, *Langmuir* **2017**, *33*, 1629.
- [35] M. Hahn, D. Rosenbach, A. Krimalowski, T. Nazarene, R. Moos, M. Thelakkat, M. A. Danzer, *Electrochim. Acta* **2020**, *344*, 136060.
- [36] M. A. Danzer, *Batteries* **2019**, *5*, 53.
- [37] M. Hahn, S. Schindler, L.-C. Triebs, M. A. Danzer, *Batteries* **2019**, *5*, 43.
- [38] Z. Samir, Y. El Merabet, M. P. F. Graça, S. S. Teixeira, M. E. Achour, L. C. Costa, *Polym. Compos.* **2018**, *39*, 1297.
- [39] M. Mours, H. H. Winter, in *Experimental Methods in Polymer Science* (Ed: T. Tanaka), Academic Press, Boston, MA **2000**, p. 495.